Molecular Therapy
Original Article

Enterovirus A71 Oncolysis of Malignant Gliomas

Xiaowei Zhang,[1] Hanzhong Wang,[1,2] Yuhan Sun,[1,4] Mi Qi,[1] Wei Li,[1] Zhiping Zhang,[1] Xian-En Zhang,[3] and Zongqiang Cui[1,4]

[1]State Key Laboratory of Virology, Wuhan Institute of Virology, Center for Biosafety Mega-Science, Chinese Academy of Sciences, Wuhan 430071, China; [2]Key Laboratory of Special Pathogens and Biosafety, Center for Emerging Infectious Diseases, Wuhan Institute of Virology, Chinese Academy of Sciences, Wuhan 430071, China; [3]National Laboratory of Biomacromolecules, CAS Center for Excellence in Biomacromolecules, Institute of Biophysics, Chinese Academy of Sciences, Beijing 100101, China; [4]University of Chinese Academy of Sciences, Beijing 100049, China

Malignant gliomas, the most lethal type of primary brain tumor, continue to be a major therapeutic challenge. Here, we found that enterovirus A71 (EV-A71) can be developed as a novel oncolytic agent against malignant gliomas. EV-A71 preferentially infected and killed malignant glioma cells relative to normal glial cells. The virus receptor human scavenger receptor class B, member 2 (SCARB2), and phorbol-12-myristate-13-acetate-induced protein 1 (PMAIP1)-mediated cell death were involved in EV-A71-induced oncolysis. In mice with implanted subcutaneous gliomas, intraneoplastic inoculation of EV-A71 caused significant tumor growth inhibition. Furthermore, in mice bearing intracranial orthotopic gliomas, intraneoplastic inoculation of EV-A71 substantially prolonged survival. By insertion of brain-specific microRNA-124 (miR124) response elements into the viral genome, we improved the tumor specificity of EV-A71 oncolytic therapy by reducing its neurotoxicity while maintaining its replication potential and oncolytic capacity in gliomas. Our study reveals that EV-A71 is a potent oncolytic agent against malignant gliomas and may have a role in treating this tumor in the clinical setting.

INTRODUCTION

Malignant gliomas are the most frequent type of primary brain tumors in adults.[1] These cancers are highly invasive, rapidly growing, and almost always fatal. The median survival is only 12–15 months for patients, despite the currently available combination approaches of surgical resection, chemotherapy, and irradiation.[2,3] Thus, the development of novel, alternative treatment options is urgently needed.

Self-replicating and tumor-selective oncolytic viruses have recently become a promising platform for cancer therapy. They are either genetically modified or have a natural propensity to infect and kill tumor cells with minimal damage to non-neoplastic tissues.[4,5] In cases where traditional approaches are unlikely to succeed, such as with malignant gliomas, virus therapy may be a novel and effective means of treatment.[6,7] Enterovirus A71 (EV-A71) is a member of the *Enterovirus* genus in the *Picornaviridae* family. Infections with EV-A71 in children younger than 5 years old predominantly cause self-limiting illnesses, although neurological manifestations are observed in a small proportion of children. In contrast, EV-A71 infections in adults rarely result in clinical symptoms.[8] The use of EV-A71 as a candidate for cancer therapy holds several favorable attributes. EV-A71 induces profound cytolytic effects during cell-to-cell infection. It replicates exclusively in the cytoplasm and does not possess oncogenes that may cause tumorigenesis. Moreover, its genome is straightforward to be engineered by reverse genetics systems.[9,10]

This study demonstrates for the first time that EV-A71 can be developed as a novel oncolytic agent against malignant gliomas. EV-A71 can infect and kill cell lines derived from malignant gliomas. EV-A71 treatment of nude mice bearing subcutaneous or intracranial glioma xenografts can induce significant inhibition of tumor progression. Furthermore, the inclusion of brain-specific microRNA-124 (miR124) response elements within the viral genome led to significant attenuation of neurovirulence but did not compromise the oncolytic activity of EV-A71. Thus, oncolysis with EV-A71 may be a potentially useful treatment for malignant gliomas.

RESULTS

EV-A71 Exerts Cytolytic Activity against Human Glioma Cells

Human neural progenitor cells (NPCs) were differentiated down a glial pathway. After induction for 21 days, differentiation of NPCs resulted in staining for the astrocytic marker glial fibrillary acidic protein (GFAP) by approximately 95% of all cells (Figure 1A). Then, the GFAP-positive human normal glial cells were used for infections. The cytolytic effects of three EVs, i.e., EV-A71, poliovirus (PV), and coxsackievirus B3 (CV-B3), were compared on human CCF malignant glioma cells and normal glial cells. For PV-infected cells, gross cell destruction and cytolysis were observed in both cells. EV-A71 infection of CCF cells led to widespread cytopathic effects, whereas it caused only limited cytolysis on normal glial cells. In contrast, nearly complete cytolysis was found in normal glia upon CV-B3 infection, but little if any changes in morphology were observed in CV-B3-infected CCF cells (Figure 1B). PV or EV-A71

Received 6 November 2019; accepted 4 April 2020;
https://doi.org/10.1016/j.ymthe.2020.04.005.

Correspondence: Zongqiang Cui, State Key Laboratory of Virology, Wuhan Institute of Virology, Center for Biosafety Mega-Science, Chinese Academy of Sciences, Wuhan 430071, China.
E-mail: czq@wh.iov.cn

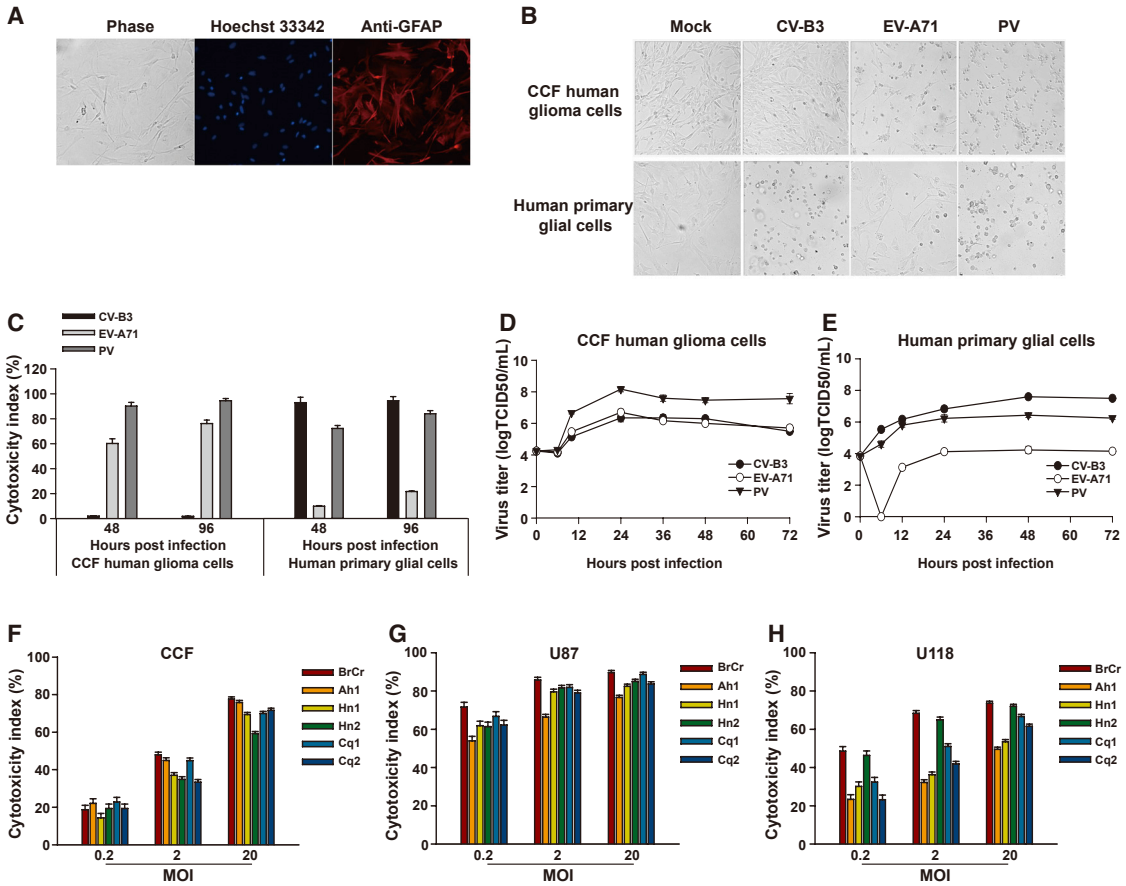

Figure 1. Cytolytic Properties of EVs against Human Glioma Cells

(A) Human NPCs differentiated for 21 days down a glial pathway resulted in staining for the astrocytic marker GFAP (red) by approximately 95% of all cells. Nuclei were stained with Hoechst 33342 (blue). Magnification, ×100. The results of one representative experiment out of three are shown. (B) Human CCF glioma cells and normal glial cells were infected with either CV-B3 Nancy, EV-A71 BrCr, or PV-1 Sabin (MOI = 1) for 48 h. Representative images were acquired under a phase-contrast microscope (magnification, ×100). (C) Human CCF glioma cells and normal glial cells were challenged with EVs (MOI = 1) for 48 h or 96 h. Cell supernatants were assessed to measure cytotoxicity. (D and E) Human CCF glioma cells (D) and normal glial cells (E) were challenged with EVs at an MOI of 1. At various times after infection, the virus titers in the culture were determined by the TCID50 assay. (F–H) EV-A71 killing of glioma cells. Three glioma cell lines, CCF (F), U87 (G), and U118 (H), were separately infected with six EV-A71 strains (BrCr, Henan1 [Hn1], Henan2 [Hn2], Chongqing1 [Cq1], Chongqing2 [Cq2], and Anhui1 [Ah1]) at MOIs of 0.2, 2, or 20 for 48 h. Cytotoxicity was assessed by an LDH assay. The results are presented as the mean ± standard deviations obtained from three independent experiments.

challenge resulted in a marked increase of cytotoxicity in CCF glioma cells, whereas only background cytolysis levels were observed following exposure to CV-B3. However, cytotoxicity in normal glial cells was substantially enhanced following infection with PV or CV-B3, whereas EV-A71 induced only limited cytolysis (Figure 1C). All three tested EVs replicated efficiently in CCF cells (Figure 1D). Notably, CCF cells have been reported to support CV-B3 replication without showing obvious cytopathogenicity.[11] Normal glial cells were efficiently infected with PV or CV-B3, whereas the peak virus yield in these cells was markedly lower for EV-A71 (Figure 1E). The ratios of maximum titer difference for viruses between CCF glioma cells and normal glial cells were calculated. A large ratio indicates a virus that selectively replicates faster in tumor cells than in normal cells and would be expected to have a stronger oncolytic profile. The ratios were approximately as follows: CV-B3, 0.06:1; EV-A71, 363.08:1; PV, 54.95:1. Together, these data suggest that EV-A71 preferentially infects and kills glioma cells relative to normal glial cells. Based on this finding, the oncolytic properties of EV-A71 against human glioma cells were investigated.

Different strains of EV-A71 were then used to assess and compare the oncolytic potential in a panel of human glioma cell lines. All glioma cell lines exhibited a dose-dependent increase in cytotoxicity upon EV-A71 infection (Figures 1F–1H). U87 (Figure 1G) and U118 (Figure 1H) glioma cells were highly susceptible to virus infection, even at low multiplicity of infection (MOI). CCF glioma cells were moderately infected by the same dose of viruses (Figure 1F). The prototype strain BrCr showed the best ability to kill the glioma cells, so we selected BrCr as the oncolytic virus candidate for further study.

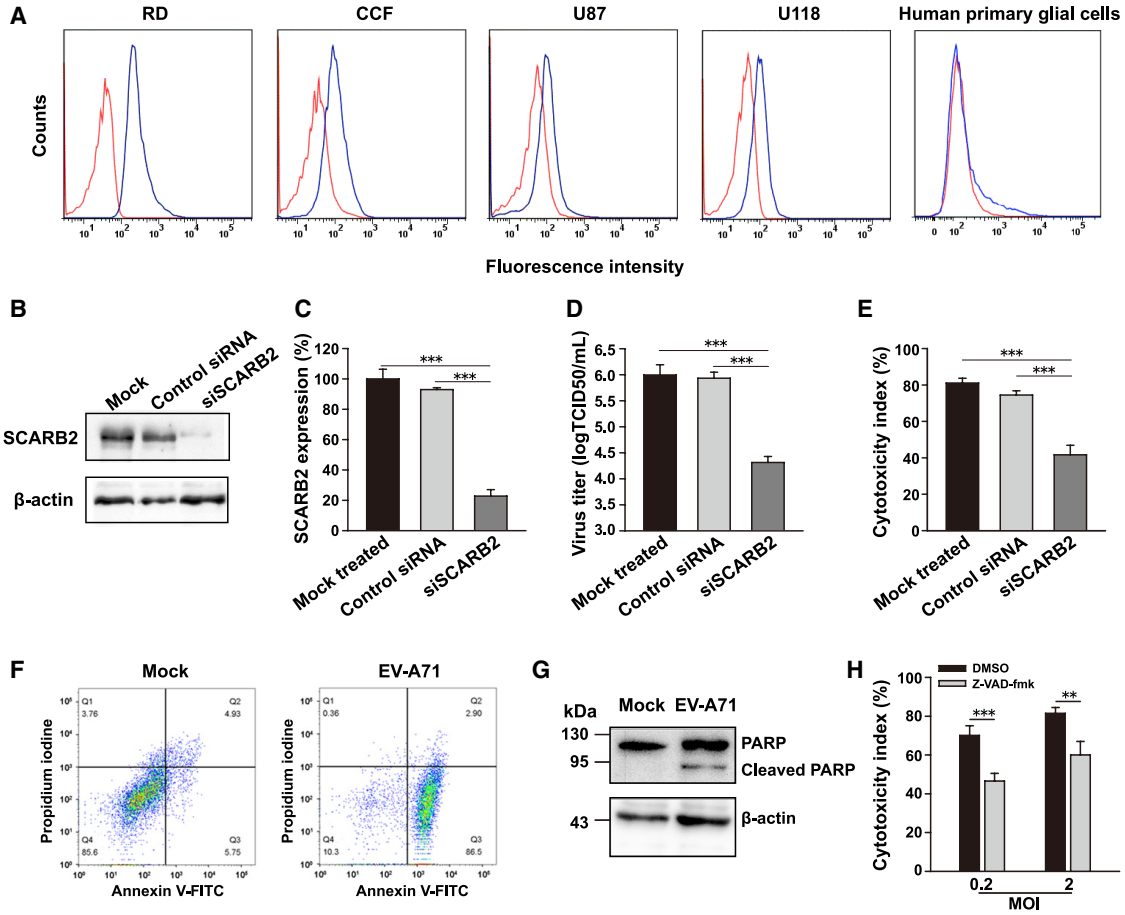

Figure 2. Roles of Virus Receptor and Apoptosis in EV-A71-Mediated Oncolysis

(A) Surface expression of EV-A71 receptor SCARB2 on human glioma cell lines and normal glial cells was quantified by flow cytometry. Representative histograms show the measured fluorescence of cells incubated with an isotype control antibody (red curves) or anti-SCARB2 antibody (blue curves). (B and C) U87 glioma cells were treated with SCARB2-specific siRNA or control siRNA. Representative immunoblot analysis of cells harvested 48 h after siRNA transfection (B). beta-actin served as a loading control. SCARB2 expression was measured by flow cytometry (C). Data are presented as the SCARB2 expression ratio relative to that in mock cells. (D and E) U87 glioma cells transfected with siRNA were infected with EV-A71 (MOI = 1) and assessed by a TCID50 assay (D) or an LDH assay (E) at 24 h postinfection. (F) U87 cells were infected with EV-A71 BrCr at an MOI of 2 for 24 h. Representative results showed that the early apoptotic population was identified as the Annexin V-FITC^{+}/PI^{-} cells. (G) Representative immunoblot analysis of cellular lysate of EV-A71-infected U87 cells. Full-length PARP (116 kDa) and an apoptotic cleavage product of PARP (89 kDa) were detected. (H) U87 cells treated with the pan-caspase inhibitor z-VAD-fmk were exposed to EV-A71. Virus-induced oncolysis was assessed by an LDH assay. Bars represent the mean ± the standard deviations of three independent experiments. **p < 0.01, ***p < 0.001.

SCARB2 Participates in EV-A71-Mediated Oncolysis

Human scavenger receptor class B, member 2 (SCARB2), was previously identified as the EV-A71 entry receptor.[12] We performed flow cytometry analyses to compare the SCARB2 expression levels. Human SCARB2 was detected on all tested glioma cell lines. Although the SCARB2 expression level was lower than that observed in RD cells , which have been used for the propagation and isolation of EVs,[13] it was worthy to note that it was higher than the SCARB2 expression level in normal glial cells (Figure 2A).

Next, we tested the role of SCARB2 in the oncolytic effects of EV-A71. U87 cells that had been treated with small interfering (si)SCARB2 were subsequently infected with EV-A71. The reduction of SCARB2 expression was confirmed by both immunoblot assay (Figure 2B) and flow cytometric analyses (Figure 2C). Knockdown did not affect cell viability (Figure S1). The virus titer was significantly reduced in siSCARB2-treated cells compared with that in untreated ($p < 0.001$) or nontargeting siRNA-treated ($p < 0.001$) cells (Figure 2D). Furthermore, the cytolytic effect of EV-A71 was significantly inhibited in the SCARB2 knockdown group, as compared with that in the untreated ($p < 0.001$) or nontargeting siRNA-treated ($p < 0.001$) group (Figure 2E). Together, these results suggest that SCARB2 participates in EV-A71-mediated oncolysis in human glioma cells.

EV-A71-Induced Apoptosis Correlates with Oncolysis in Glioma Cells

To explore the cell death mechanism in EV-A71-mediated oncolysis, U87 cells infected with EV-A71 BrCr (MOI = 2) were stained with Annexin V-fluorescein isothiocyanate (FITC) and propidium iodine (PI), followed by analysis using flow cytometry. At 24 h postinfection, a higher proportion of EV-A71-treated glioma cells belonged to the early apoptotic population, i.e., the Annexin V-FITC^{+}/PI^{-} cells, compared with the mock-infected cells (Figure 2F). Apoptosis induction was measured by the cleavage of poly (ADP-ribose) polymerase (PARP), a prominent substrate of apoptotic caspases.[14] A cleaved PARP band (~89 kDa) was clearly visible upon infection of U87 cells with EV-A71 (MOI = 0.2) (Figure 2G). The addition of z-VAD-fmk, a general caspase inhibitor, largely reduced virus-mediated cytotoxicity at an MOI of 0.2 ($p < 0.001$) or 2 ($p < 0.01$) (Figure 2H). Together, these findings suggest that EV-A71-induced apoptosis contributed to EV-A71-mediated oncolysis.

Proapoptotic PMAIP1 Induction Contributes to EV-A71-Mediated Oncolysis

To investigate further the impact of EV-A71 infection on glioma cells, we carried out transcriptome analyses (RNA sequencing [RNA-seq]). A number of differentially expressed genes were identified at 6 h after viral infection. Gene ontology enrichment analysis of regulated gene sets revealed several processes, including immune response-related and apoptosis pathways (Figure 3A). Among the apoptosis genes, phorbol-12-myristate-13-acetate-induced protein 1 (PMAIP1), which encodes a protein involved in induction of apoptosis,[15] was the top one activated by EV-A71 infection (Figure 3B). We were able to detect an approximately 24-fold increase in expression of PMAIP1. The RNA-seq data were then validated by both qPCR and western blot (WB) assays. EV-A71 treatment led to a significant increase in PMAIP1 mRNA expression (Figure 3C). Immunoblotting also revealed that the PMAIP1 protein was markedly induced after EV-A71 infection (Figure 3D). Based on these results, it is hypothesized that PMAIP1 may play a role in EV-A71-induced cell death in glioma cells. To test this, PMAIP1-specific siRNA was utilized to knock down its expression in the U87 cells (Figure 3E). Of note, a reduction in PMAIP1 levels significantly decreased EV-A71-induced cytotoxicity ($p < 0.01$) (Figure 3F). These data indicate that proapoptotic PMAIP1 is involved in EV-A71-mediated oncolysis in glioma cells.

EV-A71 Exhibits Potent Antitumor Activity in Glioma Xenografts

We next analyzed the oncolytic effects of EV-A71 *in vivo* using a subcutaneous malignant glioma xenograft model. Compared with control vehicle treatment, tumor growth was substantially retarded after treatment with EV-A71. Representative pictures taken at the time of sacrifice clearly show the gross therapeutic effect (Figure 4A). At day 25, the last day in which all animals were alive, the mean tumor volume of the control group exceeded 850 mm^3 (range 546–1,245 mm^3), whereas the mean tumor volume in the EV-A71 therapy group was <85 mm^3 (range 11–225 mm^3) ($p < 0.001$) (Figure 4B). H&E staining of the remaining tumor mass demonstrated significant tumor cell loss in the EV-A71 therapy group. The bulk of the tumor no longer had the appearance of a proliferating tumor, in contrast with the dense, hypercellular architecture of vehicle-treated tumors (Figure 4C). Immunohistochemistry (IHC) for EV-A71 protein revealed a viral presence in the residual tumor cells from EV-A71-treated animals (Figure 4D). Apoptotic changes, as detected by a terminal deoxynucleotidyl transferase-mediated 2′-deoxyuridine 5′-triphosphate (dUTP) nick end labeling (TUNEL) assay, were observed in the EV-A71-treated xenograft tumor cells (Figure 4E). There was no obvious gross toxicity based on body weight measurements over 25 days (Figure S2). None of the EV-A71-treated animals developed neurological disorders, and the mice were sacrificed due to tumor growth. All of the mice in the vehicle-treated group reached the endpoint due to massive tumors; a significant survival benefit (95% confidence interval [CI] = 25.10–41.56, $p < 0.001$) was observed in EV-A71-treated mice (Figure 4F).

To determine whether EV-A71 exhibits oncolytic activity against human glioma cells growing in mouse brains, U87 glioma cells were xenotransplanted into the right cerebral hemispheres of mice, and 7 days later, EV-A71 was inoculated into the same stereotactic coordinates initially used to inject the glioma cells. Untreated mice became moribund within 33–45 days after tumor induction (average, 38.3 days). EV-A71 treatment produced a significant increase in median survival (95% CI = 15.36–31.98, $p < 0.001$), with approximately 33% of the tumor-bearing mice surviving to 70 days, at which point, the long-time survivors were euthanized (Figure 4G). At 45 days post-tumor implantation, H&E histological examination of representative brains from moribund, untreated mice revealed large, space-occupying tumors; in contrast, the glioma xenografts in mice that had received an inoculation of EV-A71 were dramatically smaller (Figure 4H). EV-A71 viral protein was detected by IHC in microscopic residual tumor cells in virus-treated mice (Figure 4I). In addition, we detected marked TUNEL staining, a marker of apoptosis, in the EV-A71-treated tumor residues. A few scattered TUNEL signal-positive cells were detected in the vehicle-treated tumor masses (Figure 4J). These data suggest that EV-A71 has the ability to cause glioma regression *in vivo*.

EV-A71 Accommodates miR124-Target Elements to Ameliorate Its Potential Neurotoxicity

Safety is a pivotal concern for the application of oncolytic therapy, especially in the treatment of sensitive tissue, such as the brain. To restrict the tropism of viruses, tissue-specific microRNAs (miRNAs) have been exploited.[16] Recent studies found that miR124 is enriched within normal brain tissues, whereas it is nearly absent in all grades of gliomas.[17] To alleviate potential neurotoxicity of EV-A71, we engineered de-targeted viruses, designated as EV-A71-miR124T, by inserting miRNA target sequences (miRTs) for miR124 immediately preceding the coding region. We also generated a control virus, called EV-A71-CelTCON, by inserting target sequences of a *Caenorhabditis elegans*-derived miR39, which has no identified target in mammalian cells[18] (Figure 5A). The capability of miRT-containing viruses to replicate *in vitro* was evaluated in Vero cells (an African green monkey kidney cell line), which do not express miR124.[19] Both

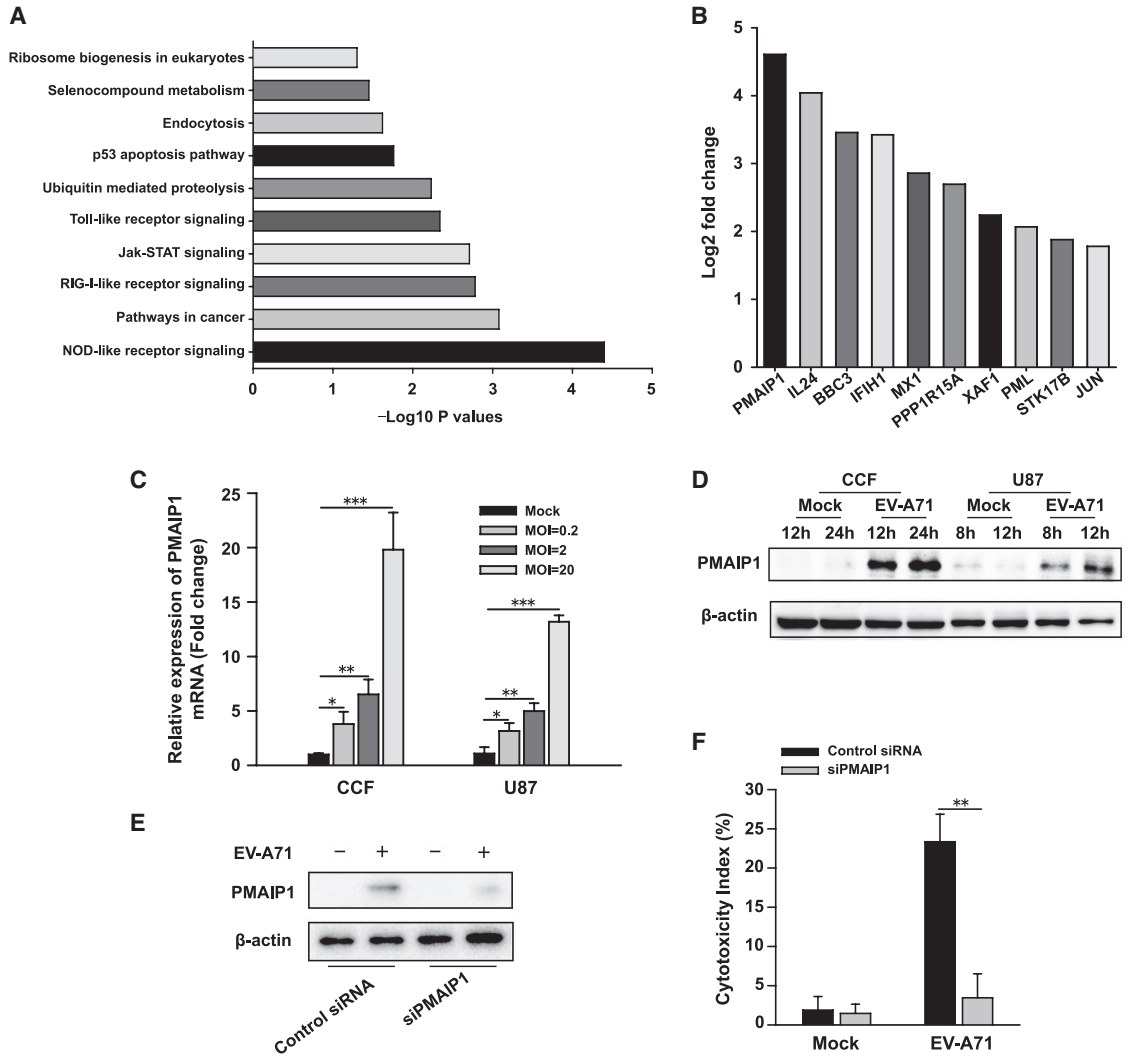

Figure 3. PMAIP1 Induction Is Involved in EV-A71-Mediated Oncolysis

(A) RNA-seq analyses of EV-A71-infected and mock-infected human glioma cells. Genes with significant differences in expression were subjected to GO analyses. The typical 10 most significant terms are shown. The −log10 p values are indicated by bar plots. (B) RNA expression analysis of RNA-seq results. Bar plots indicate induction of apoptosis-related genes in EV-A71-infected glioma cells, as compared with mock cells. (C and D) EV-A71 increases PMAIP1 mRNA and protein levels in human glioma cells. Total RNA and whole-cell lysates were prepared from CCF or U87 cells treated with EV-A71 BrCr or vehicle as control. (C) PMAIP1 mRNA expression was quantified by real-time PCR, 6 h after virus treatment with the indicated MOIs. (D) Immunoblot analysis was performed for PMAIP1 protein expression after treatment with EV-A71 at an MOI of 2 for indicated times. beta-actin was used as control for protein loading. One representative image of three experiments is shown. (E and F) Knockdown of PMAIP1 reduces EV-A71-mediated oncolysis. U87 glioma cells were treated with siRNA for 48 h. Cells were then infected with EV-A71 (MOI = 2) for an additional 8 h. (E) Reduced NOXA expression was confirmed by immunoblotting. (F) EV-A71-induced oncolysis was measured by an LDH assay. Bars represent the mean ± the standard deviations of three independent experiments. *$p < 0.05$, **$p < 0.01$, ***$p < 0.001$.

miRT-containing viruses exhibited identical growth kinetics compared with those of unmodified virus (Figure 5B). Sequence analyses indicated that both recombinant miRT-containing viruses were genetically stable in cells, and no changes were observed in the miRNA-target insertions.

The specificity of miRNA-mediated regulation of viral tropism was determined by analyzing virus replication and cell viability in EV-A71-infected Vero cells after their transfection with miRNA mimics. The EV-A71-miR124T virus titer was decreased in a dose-dependent manner when cells were transfected with 10–200 nM miR124 mimic (Figure 5C). At the highest concentration of 200 nM, the miR124 mimic markedly protected cells from viral lysis by EV-A71-miR124T as compared with that by EV-A71 BrCr ($p < 0.001$), whereas the cytotoxicity of EV-A71-CelTCON was unaffected. The EV-A71-miR124T virus titer was significantly decreased in the

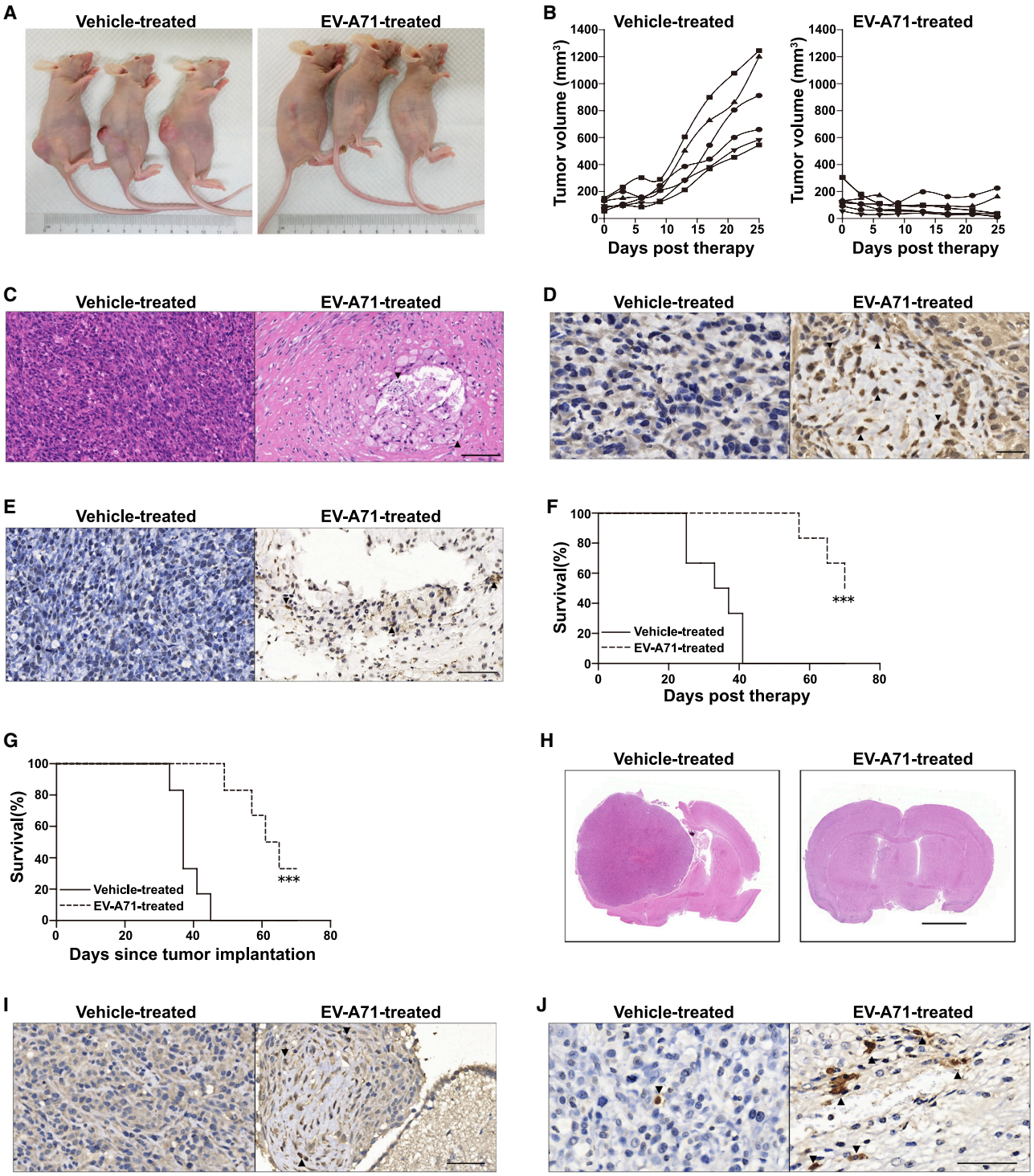

Figure 4. EV-A71 Oncolytic Activity against Glioma Xenografts

(A and B) Nude mice bearing subcutaneous U87 tumors were treated with intratumoral injection of vehicle or EV-A71. (A) Representative photographs of the xenograft tumor on day 25 post-therapy are shown. (B) The tumor burden was monitored by calculating the tumor volume versus time using calipers. (C) Representative H&E staining of the remaining tumor mass at 25 days post-treatment with vehicle or EV-A71. Black triangles indicate significant tumor cell loss. Scale bar, 100 μm. (D) Representative IHC analysis of EV-A71 proteins in paraffin-embedded sections. Black triangles indicate positive staining for virus protein 2B. Scale bar, 20 μm. (E) Representative apoptosis

(legend continued on next page)

presence of the miR124 mimic ($p < 0.001$), whereas the EV-A71-CelTCON virus titer was not affected. As expected, neither miRT EV-A71 had any substantially reduced cytotoxicity or replication in cells transfected with the miRNA mimic control (Figures 5D and 5E).

EV-A71 was previously shown to cause asymptomatic infection in adult immunodeficient mice.[20] As expected, intracerebral injection of CD1 nude mice with high titers of EV-A71 BrCr (10^7 50% tissue culture infectious dose [TCID50]) did not cause any morbidity and mortality over a 14-day period. Thus, 1-day-old suckling mice, which are the age group most susceptible to EV-A71 infection[21] and show a robust pattern of miR124 expression in their brains,[22] were intracerebrally injected with either EV-A71 BrCr or EV-A71-miR124T to investigate the *in vivo* neurotoxicity. EV-A71 BrCr infection led to a mortality rate of 25% (2/8) over a 14-day period, whereas no deaths occurred following infection with EV-A71-miR124T (Figure 5F). Suckling mice intracerebrally infected with EV-A71-miR124T had significantly lower viral titers than those infected with EV-A71 BrCr ($p < 0.001$) at 2 days postinoculation. Infectious virus was not detected in the large majority of EV-A71-miR124T-infected mice (Figure 5G).

To determine whether miR124-sensitive EV-A71-miR124T is attenuated in primary human neurons (HNs) or mouse neurons (MNs) physiologically expressing miR124,[23] we examined infection efficiency and cellular toxicity of EV-A71-miR124T in primary neurons compared to those of parental EV-A71 BrCr. As shown in Figure 5H, immunostaining of the viral antigen in HNs or MNs infected with EV-A71-miR124T was diminished compared to that observed for cells infected with EV-A71 BrCr. Moreover, EV-A71-miR124T infection in neurons was strongly attenuated in terms of virus replication compared to EV-A71 BrCr (Figure 5I). Measurement of lactate dehydrogenase (LDH) efflux further showed that EV-A71-miR124T infection caused significantly reduced cell damage in neurons (Figure 5J). These results indicate that oncolytic EV-A71 can be engineered to be sensitive to the presence of the brain-enriched miR124.

miR124-Sensitive EV-A71 Has Oncolytic Activity against Gliomas

U87 cells were infected with EV-A71 BrCr or EV-A71-miR124T to test the oncolytic activity. Both viruses produced similar viral growth curves, suggesting they were both capable of efficiently infecting U87 cells (Figure 6A). Moreover, no significant differences in cytolytic properties were detected between the unmodified EV-A71 BrCr and miRT-containing viruses using an LDH assay (Figure 6B). We then compared the oncolytic efficacy of EV-A71-miR124T and parental EV-A71 BrCr in mice bearing subcutaneous tumors. A similar oncolytic effect with strongly retarded tumor growth was observed after treatment with either EV-A71 BrCr or EV-A71-miR124T ($p = 0.94$), as compared with vehicle controls (EV-A71 BrCr versus vehicle, $p < 0.001$; EV-A71-miR124T versus vehicle, $p < 0.001$) (Figures 6C–6E). The oncolytic activity of EV-A71-miR124T compared with that of EV-A71 BrCr was then measured on intracranial glioma xenografts. Notably, treatment with either EV-A71 BrCr (95% CI = 14.48–31.52, $p < 0.001$) or EV-A71-miR124T (95% CI = 14.80–30.87, $p < 0.001$) markedly extended the lifespan of tumor-bearing mice. Notably, there was no significant difference in the survival time of mice in which the tumor was inoculated with parental EV-A71 BrCr and those inoculated with EV-A71-miR124T ($p = 0.82$) (Figure 6F).

Animals were killed on days 45 post-tumor implantation, and serial brain sections from EV-A71-miR124T-infected, intracranial, glioma-bearing mice were examined simultaneously for parallel miR124/viral protein localization and histological evaluation. Fluorescence *in situ* hybridization (FISH) analyses indicate that miR124 (green) was readily detectable in nontumor-bearing areas of the brain. By contrast, the IHC or TUNEL findings showed that EV-A71-positive or apoptotic cells were largely restricted to the tumor mass rather than normal tissues (Figure 6G). Together, the inclusion of brain-specific miR124 response elements led to significant attenuation of neurovirulence but did not compromise the oncolytic activity of EV-A71 against gliomas with low miR124 expression.

DISCUSSION

Here, we identified EV-A71 as a novel oncolytic agent. It has been reported that local self-amplification is one of the mainstays of oncolytic virus therapy. Viruses selectively replicating faster in tumor cells than in normal cells would be expected to have a stronger oncolytic profile.[24] EV-A71 had a relative higher level of virus replication in glioma cells than in normal cells. Therefore, the oncolytic potential of EV-A71 against gliomas was investigated further in this study. EV-A71 showed therapeutic efficacy against gliomas, and oncolysis with it may be a potentially useful treatment for malignant gliomas.

The tropism of oncolytic viruses is determined by viral receptor expression on target tumors.[25] Our results show that the tested glioma cell lines express SCARB2, an entry receptor for EV-A71. Downregulation of its expression not only significantly suppressed virus replication but also attenuated the oncolytic efficacy of EV-A71. Notably, normal glial cells, which were relatively refractory to EV-A71 infection, expressed lower levels of SCARB2. Previous

analysis in vehicle- or EV-A71-treated subcutaneous glioma xenografts. Black triangles indicate significant features of apoptotic cell death. Scale bar, 50 μm. (F) Overall survival of mice was assessed using the Kaplan–Meier survival log rank test. The animals were sacrificed by cervical dislocation once the implanted tumor size exceeded 15 mm in any direction, which was considered the humane endpoint of survival data. (G) Nude mice bearing intracranial U87 tumors were treated with intratumoral injection of vehicle or EV-A71 BrCr. Overall survival was analyzed by the Kaplan–Meier survival log rank test. (H) Representative coronal H&E-stained sections of nude mouse brains. The tumors of mock-treated moribund animals encompassed almost the entire hemisphere with marked hypercellularity, whereas only microscopic residual tumor cells remained in EV-A71-treated animals at the same time. Scale bar, 2 mm. (I) Representative IHC detection of EV-A71 protein 2B (marked with black triangles). Scale bar, 50 μm. (J) Representative apoptosis analysis in intracranial glioma xenografts as detected by TUNEL staining (marked with black triangles). Scale bar, 50 μm. ***$p < 0.001$.

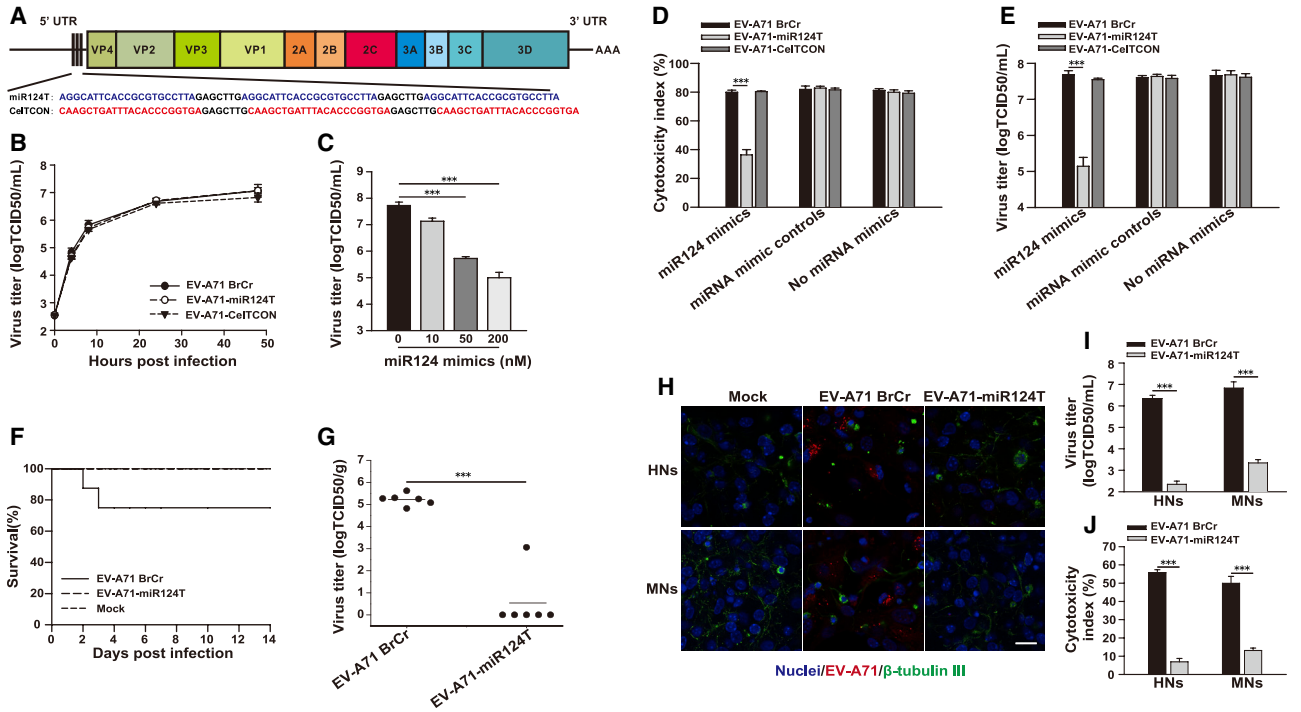

Figure 5. Construction and Characterization of Recombinant miR124-Regulated EV-A71

(A) Schematic representation of miRT EV-A71. Three tandem copies of sequences complementary to miRNAs were inserted into the viral genome. The brain-specific miR124-target sequence (miR124T, blue) and *Caenorhabditis elegans*-derived miR39-target sequence (CelTCON, red) are shown, with spacer elements in black. (B) Replication kinetics of EV-A71 BrCr, EV-A71-miR124T, or EV-A71-CelTCON in Vero cells (MOI = 1). (C) The EV-A71-miR124T virus titers were determined after transfection with increasing doses of miR124 mimics (MOI = 20). (D) Vero cells transfected with 200 nM miRNA mimics were subsequently infected with EV-A71 BrCr, EV-A71-miR124T, or EV-A71-CelTCON (MOI = 20), and the cytotoxicity was determined at 24 h postinfection by an LDH assay. (E) Viral titers in the supernatants of the miRNA mimic-treated cells were determined. Bars represent the mean ± standard deviations of three independent experiments. (F) Suckling mice were injected intracerebrally with vehicle or 10^7 TCID50s of EV-A71 BrCr or EV-A71-miR124T. The overall survival of mice was assessed. (G) Viral titers within the brain at 2 days postinjection were determined. Individual viral load values are plotted along with the mean viral load (solid line). (H–J) Primary human neurons (HNs) or mouse neurons (MNs) were infected with EV-A71 BrCr, EV-A71-miR124T at an MOI of 10 for 48 h or mock-treated, respectively. (H) Viral antigen (red) and β-tubulin III (green) were detected using IFA. Cell nuclei (blue) were counterstained with Hoechst 33342. Scale bar, 20 μm. The results of one representative experiment out of three are shown. (I) Virus titers in the culture were determined by the TCID50 assay. (J) Cytotoxicity was assessed by an LDH assay. The results are presented as the mean ± standard deviations obtained from three independent experiments. ***$p < 0.001$.

work found that SCARB2 expression was upregulated in tumor sections of malignant gliomas compared with normal brain samples.[26] The discriminatory expression of SCARB2 may facilitate selective targeting for EV-A71 against malignant gliomas rather than normal brain cells; this warrants further study. In addition to SCARB2, human P-selectin glycoprotein ligand-1 (PSGL-1) was reported as a candidate receptor for EV-A71.[27] Several EV-A71 strains (PSGL-1-binding strain EV-A71-PB) bind to PSGL-1, but other strains, including EV-A71 BrCr, used in this study, do not.[28] Thus, PSGL-1 should not contribute to oncolysis of gliomas mediated by EV-A71 BrCr.

EV-A71 is a potent apoptosis inducer.[29] We demonstrated here that EV-A71 could stimulate the cleavage of PARP, a prominent substrate of apoptotic caspases in glioma cells. Furthermore, caspase inhibition effectively ameliorated virus-induced oncolysis. Treatment with EV-A71 led to obvious glioma cell apoptosis in both subcutaneous and intracranial xenograft models. One of the features of malignant gliomas is their resistance to cellular apoptosis induced by treatments, such as radiation and chemotherapy.[30] Thus, the ability of EV-A71 to induce apoptosis in malignant glioma cells may be an attractive property for its use in the treatment of this type of apoptosis-resistant tumor. PMAIP1 plays a role in EV-A71-induced oncolysis, as siRNA-mediated knockdown of PMAIP1 significantly inhibited virus-induced cell death. Induction of PMAIP1 has also been shown to be involved in reovirus or Sendai virus-induced oncolysis.[31,32] Besides, a combination of reovirus infection and proteasomal inhibition led to enhanced PMAIP1 induction and therefore, the anti-myeloma effects.[32] It has been reported that treatment with the US Food and Drug Administration (FDA)-approved proteasome inhibitor bortezomib led to induction of PMAIP1, accompanied by increased levels of activated caspase in cancer cells.[33] The identification of the molecular basis that modulates inductions of both PMAIP1 and active caspase upon treatment with EV-A71 alone or the combination of EV-A71 and bortezomib may further augment the antitumor efficacy of oncolytic virus therapy.

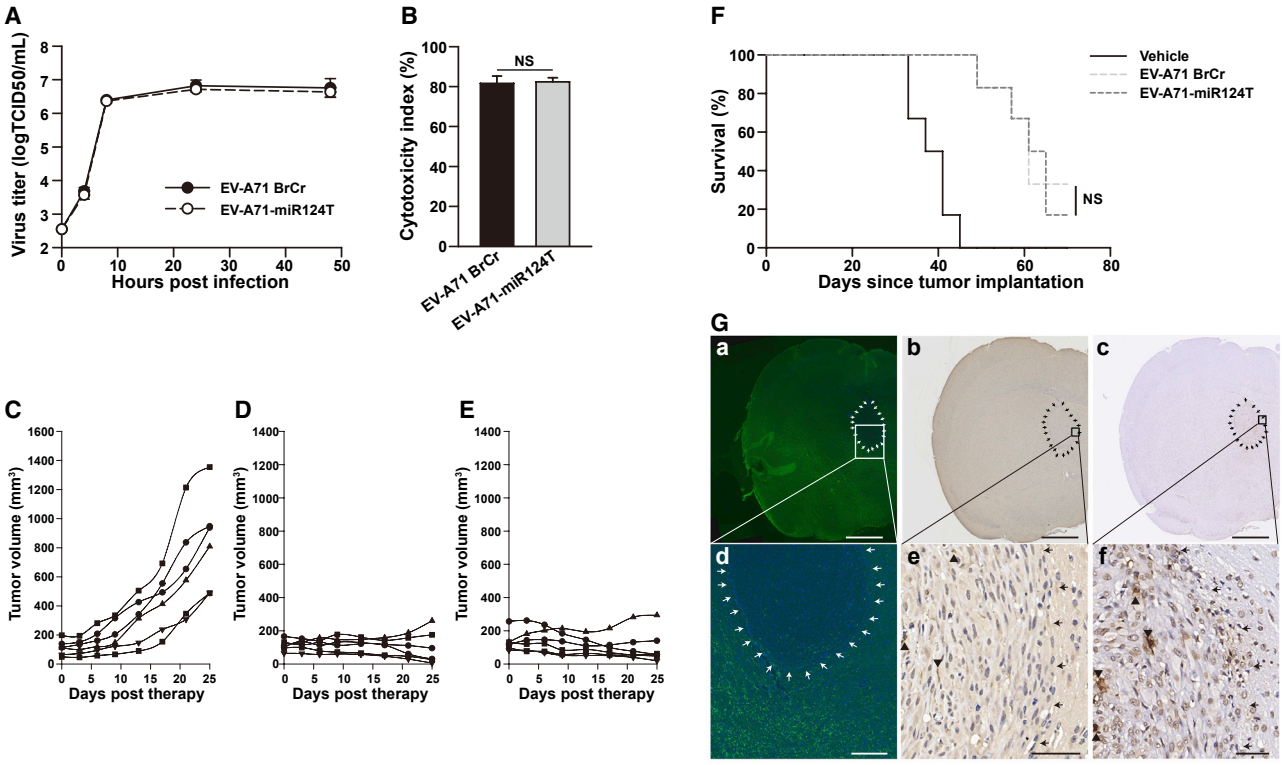

Figure 6. Antitumor Activity of miR124-Sensitive EV-A71 against Gliomas

(A) Replication kinetics of EV-A71 BrCr and EV-A71-miR124T in U87 cells (MOI = 1). (B) U87 cells were infected with virus (MOI = 2) for 48 h. Cytotoxicity was then assessed by an LDH assay. (C–E) Nude mice bearing subcutaneous U87 tumors were treated with intratumoral injection of vehicle (C), EV-A71 BrCr (D), or EV-A71-miR124T (E). Tumor burden was monitored by calculating tumor volume versus time using calipers. (F) Nude mice with intracranial glioma xenografts were treated with vehicle, EV-A71 BrCr, or EV-A71-miR124T. The number of surviving animals was recorded daily and plotted against time. Significance was analyzed by a Kaplan–Meier survival log rank test. (G) Representative results of parallel staining patterns for miR124, viral protein, and virus-induced apoptotic cells in mouse brain after EV-A71-miR124T treatment. Serial sections in the left column were hybridized with the miR124-specific LNA miRCURY probe. Sections in the middle and right columns are consecutive tissue sections of those on the left, and EV-A71-positive cells and apoptotic cells were detected by IHC and TUNEL assay, respectively. Low (a–c) and high (d–f) power views of brain sections. Arrows demarcate approximate edges of the tumor mass where it interfaces with normal tissue. FISH analyses indicate that miR124 (green) is largely restricted in nontumor-bearing areas of the brain. Viral protein-positive and TUNEL-positive cells are marked with black triangles within the tumor. Scale bars, 1 mm (a–c); 200 μm (d); 50 μm (e and f). NS, not significant.

miRNAs are small, endogenous RNAs that mediate the post-transcriptional regulation of gene expression in multicellular eukaryotes.[34] Differential miRNA expression in neoplastic tissues is an emerging hallmark of cancer, with various miRNAs found to be downregulated in malignant cells.[35,36] miR124 is a brain-enriched miRNA that has been shown to be scarcely expressed or absent in gliomas.[17] Here, we exploited the differential expression of miR124 to control the replication specificity of EV-A71 in malignant glioma cells. Intracerebral infection with EV-A71-miR124T led to no death in mice, whereas wild-type EV-A71 BrCr infection caused 25% mortality. Combined with data showing that EV-A71-miR124T replication was attenuated in mice brain and primary neurons *in vitro*, it can be speculated that EV-A71-miR124T, engineered to become targets of neuron-specific miR124, were significantly compromised in their ability to replicate in the CNS, leading to reduced neurovirulence in infected animals. Our results demonstrate that miR124-mediated suppression of virus replication can lead to significant attenuation of neurovirulence of EV-A71 in brain tissues. Even though it is attenuated in the presence of miR124 in normal brain, EV-A71-miR124T retained full efficacy against both glioma cells and xenografts with downregulated expression of miR124. This provides a proof of concept that tropism restriction by tissue-specific miRNAs can be adapted to regulate EV-A71 viral replication to maximize tumor specificity. The constructed attenuated form of EV-A71 with lower adverse effects will facilitate the transition of EV-A71 to further experimental and clinical trials, such as for the treatment of primary gliomas or tumor-initiating cells.

Of course, this study still has some limitations. The *in vivo* efficacy data reported in this study were obtained using immune-deficient nude mice. Antiviral immune responses, such as induction of type I interferons (IFNs) or neutralizing antibodies, were once proposed as potential obstacles to oncolytic therapy. However, some studies raise the possibility that type I IFN pathway modulators, in

combination with an IFN-sensitive oncolytic virus, could be used to enhance therapeutic efficacy.[37,38] This strategy might also be considered for oncolytic EV-A71 if it was sensitive to type I IFNs. The antitumor effect displayed by oncolytic viruses is not only related to their intrinsic oncolytic effect but also to the triggering of an immune response. Evidence has been accumulating that antiviral immunity can activate the immune response against the tumors and improve oncolytic virus therapy.[39,40] To enhance further the efficacy of oncolytic EV-A71, multiple viral administrations and a combination of EV-A71 with chemotherapy, radiotherapy, or immune modulators[41] merit further studies for future clinical translation.

In conclusion, this study provides evidence that EV-A71 possess potent oncolytic activity against malignant gliomas. The potential neurotoxicity of EV-A71 can be greatly reduced by the insertion of brain-specific miR124 response elements. This altered phenotype, combined with a natural tropism for malignant glioma cells that express SCARB2 and an inherent apoptosis-inducing property, suggests that oncolysis with EV-A71 may be a potentially useful treatment for malignant gliomas.

MATERIALS AND METHODS

Ethics Statement

All animal experimental procedures were performed in accordance with the guidance of the Institutional Animal Care and Use Committee of Wuhan Institute of Virology, Chinese Academy of Sciences. All surgeries were performed under general anesthesia, and all efforts were made to minimize the number of animals used and their suffering.

Cell Lines and Cultures

U87 (a human malignant glioma cell line; ATCC HTB-14), U118 (a human malignant glioma cell line; ATCC HTB-15), and RD (a human rhabdomyosarcoma cell line; ATCC CCL-136) cells were grown in DMEM. CCF-STTG1 (a human malignant glioma cell line; ATCC CRL-1718) cells were grown in RPMI 1640. Vero (an African green monkey kidney cell line; ATCC CCL-81) cells were cultured in minimum essential medium (MEM). All culture media were supplemented with 10% fetal bovine serum (FBS), 2 mM L-glutamine, 100 U/mL penicillin, and 100 mg/mL streptomycin (Life Technologies). Notably, U87 ATCC cells used in our study, as well as that of others, are of different genetic origin from U87 Uppsala cells. Nevertheless, the ATCC-derived U87 is still considered to be a bonafide human glioblastoma cell line on the basis of genetic analysis. Human NPCs were obtained from human fetal brain tissue and differentiated into primary cells of glial lineage (human primary glial cells), as described previously.[11,42] Briefly, NPCs were maintained in DMEM–F-12 medium, supplemented with 10% FBS, gentamicin (50 μg/mL), and amphotericin B (1.5 μg/mL). After 21 days of differentiation, the cell in the cultures were approximately 95% GFAP positive and used for the following experiment. Primary HNs isolated from human brains were obtained from Sciencell Research Laboratories (ScienCell) and maintained in neuronal medium supplemented with neuronal growth supplement (ScienCell), according to the manufacturer's instructions. Primary MNs, prepared from 1-day-old suckling mice brain, were obtained from Procell Life Science & Technology (Procell) and cultured in neurobasal medium containing a B-27 supplement (Gibco). HNs and MNs were characterized by immunofluorescence with neuron-specific β-tubulin III antibody (T8578; Sigma).

Viruses

A prototype strain of EV-A71 (EV-A71 BrCr; GenBank: U22521) was obtained from the Institute of Medical Biology, Chinese Academy of Medical Science. The isolated strains of EV-A71, namely Henan1 (Hn1; GenBank: GU196833), Henan2 (Hn2; GenBank: GQ994992), Chongqing1 (Cq1; GenBank: GQ994989), Chongqing2 (Cq2; GenBank: GQ994990), and Anhui1 (Ah1; GenBank: GQ994988), were provided courtesy of G.H. Chang from the Beijing Institute of Microbiology and Epidemiology. The PV type 1 Sabin strain (GenBank: AY184219) was kindly provided by Y.Z. Jiang from the Hubei Provincial Center for Disease Control and Prevention. The CV-B3 strain Nancy (GenBank: JX312064) was provided courtesy of Z.Q. Yang from Wuhan University. The virus titer was measured as the TCID50 in Vero cells using the Reed-Muench formula.

Virus Infection

Cell monolayers were infected with EVs at the MOI indicated below for 1 h. Inoculated cell cultures were washed three times with phosphate-buffered saline (PBS) and then replenished with complete medium. Cytopathic effects were judged using phase-contrast microscopy. Culture supernatants and cell monolayers were harvested at the indicated times for further analysis.

LDH Assay

Virus-induced cytotoxicity was assessed by the release of the cytoplasmic enzyme LDH, which was measured using a commercial kit (Beyotime), as described previously.[11] Virus-induced cytotoxicity is expressed as a percentage of the maximum LDH release induced by lysis buffer treatment.

Immunofluorescence Assay (IFA)

To detect EV-A71 antigen in infected cells, cell monolayers were infected with EV-A71 BrCr or EV-A71-miR124T at an MOI of 10 for 48 h. Cells were fixed in 4% paraformaldehyde (PFA)–PBS for 15 min at room temperature, permeabilized with 0.2% Triton X-100–PBS for 10 min, and blocked in PBS with 2% normal donkey serum for 1 h at room temperature. Cells were subsequently incubated with the mouse anti-β-tubulin III (neuronal) antibody (T8578; Sigma) and rabbit anti-EV-A71 VP1 polyclonal antibody (GTX132339; GeneTex) at room temperature for 1 h. The cells were rinsed three times with PBS and incubated for 1 h with the secondary antibodies Alexa 488-conjugated donkey anti-mouse immunoglobulin G (IgG) and Alexa 594-conjugated donkey anti-rabbit IgG (Thermo Fisher Scientific). After washes, cell nuclei were counterstained with Hoechst 33342. Cells were visualized under a Dragonfly spinning confocal system (Andor Technology), and data were obtained and processed using Andor Fusion and Imaris imaging software, respectively. For IFA

to detect the astrocyte maker GFAP, cells were fixed and blocked as described above. The primary antibody used was rabbit anti-GFAP polyclonal antibody (BM4287; Boster).

pEV-A71-miRT Plasmids

The infectious clone pEV-A71 BrCr[43] was used as the starting material for genetic manipulation. We cloned three copies of miRNA-target sequence (miR124-target sequence: 5′-AGGCATTC ACCGCGTGCCTTA-3′; *Caenorhabditis elegans*-derived miR39-target sequence: 5′-CAAGCTGATTTACACCCGGTGA-3′) into the location between the 5′ untranslated region (UTR) and the coding sequences using splice-overlap extension PCR.[18] The integrity of the regions flanking the integrated miRT was verified by sequencing.

Recombinant EV-A71-miRT Viruses

Viral RNA was produced using a RiboMax large-scale RNA production system T7 kit (Promega), according to the manufacturer's instructions. The RNA was then transfected into Vero cells to rescue recombinant viruses using the TransIT mRNA transfection reagent (Mirus Bio). The resulting progeny viruses were passaged three times to obtain suitable viral titers. The integrity of the targets was verified by sequencing.

miRNA Mimic Transfection

miRNA mimics of hsa-miR124-3p (miRBase: MIMAT0000422) and micrON miRNA mimic control, which had no identified target in mammalian cells, were purchased from RiboBio. The miRNA mimics were transfected at a final concentration of 10, 50, or 200 nM using the HiPerFect transfection reagent (QIAGEN), following the manufacturer's instructions. At 4 h post-transfection, the cells were infected with EV-A71 BrCr at an MOI of 2. At 24 h postinfection, the virus-induced cytotoxicity was measured, and the virus titer was determined.

Annexin V-FITC/PI-Stained Fluorescence-Activated Cell Sorting (FACS)

After EV-A71 BrCr infection, apoptotic cells were quantified using an Annexin V-FITC/PI double-staining kit (Beyotime), according to the manufacturer's instructions. Cell samples were analyzed using the BD LSR Fortessa and FACSDiva software (BD Biosciences).

FACS Analysis of SCARB2 Expression

Cell-surface expression of SCARB2 was analyzed on both glioma cells and normal glial cells by performing flow cytometry, as described previously.[11] Briefly, dispersed cells were incubated with 0.5 μg of anti-SCARB2 (NB400-102; Novus Biologicals) or corresponding isotype control antibody (NBP2-24891; Novus Biologicals) for 30 min at 4°C. Cells were washed with PBS containing 2% FBS and pelleted by centrifugation before resuspension in solution containing 0.5 μg of FITC-conjugated donkey anti-rabbit IgG antibody (Poly4064; Bio-Legend). Following an incubation of 30 min at 4°C in the dark, the cells were washed twice before flow cytometric analysis (FACS LSRFortessa; BD Biosciences).

RNA-Seq Analyses

Total RNA samples from CCF glioma cells after EV-A71 BrCr or mock infection (MOI = 2) were used for RNA-seq analyses by BGI-Shenzhen using the Illumina HiSeq 2000 system. The gene-expression level was calculated and normalized by using the TPM (the number of transcripts per million clean tags) method.[44] False discovery rate (FDR) $\leq$ 0.001 and the absolute value of log2 ratio $\geq$ 1 were used as the threshold to judge the significance of the differential gene expression.[45] Differentially expressed genes were mapped to Gene Ontology (GO) terms in the GO database (http://www.geneontology.org/) by a hypergeometric test, and the Bonferroni-corrected p value $\leq$ 0.05 was used as the threshold.[46] The accession number for RNA-seq data reported in this paper is GEO: GSE136330.

Quantitative Real-Time PCR

Total RNA was extracted from the cells using the Omega HP total RNA Isolation Kit (Omega Bio-Tek). Quantification of the mRNA was performed with real-time PCR (CFX96 Real-Time PCR System; Bio-Rad) using primers specific for human PMAIP1[47] and a One Step SYBR PrimeScript RT-PCR Kit (TaKaRa). The data acquisition and analysis were carried out by Bio-Rad CFX Manager software. Relative expression of PMAIP1 was normalized with β-actin. The data are expressed as the relative fold increase of the stimulated over the mock control group.

RNA Interference (RNAi)

RNAi was performed using the previously described human SCARB2-specific siRNA,[13] PMAIP1-specific siRNA,[48] or a control-nontargeting siRNA (RiboBio). Cells were transfected with siRNA using the HiPerFect transfection reagent, according to the manufacturer's protocols. Some of these cells were harvested at 48 h post-transfection for flow cytometry analysis, as described above. Others were infected with EV-A71 BrCr at an MOI of 1 and further incubated for indicated times at 37°C. Culture supernatants and cell monolayers were then harvested for further analysis.

Western Blot Analysis

Cell lysate samples were resolved by SDS-PAGE and immunoblotted as described previously.[49] The primary antibodies against PARP (46D11; CST), SCARB2 (NB400-102; Novus Biologicals), PMAIP1 (A9801; ABclonal), and β-actin (2D4H5; Proteintech Group) were used. β-actin served as a loading control.

Apoptosis Inhibition Assay

For apoptosis inhibition assays, U87 glioma cells were pretreated with the pan-caspase inhibitor, z-VAD-fmk, at a final concentration of 200 μM, as described previously,[50] followed by exposure to EV-A71 at an MOI of 0.2 or 2 for 1 h. The cells were then maintained in DMEM with 2% FBS containing 200 μM z-VAD-fmk for an additional 24 h. Virus-induced cytotoxicity was measured as described above.

Attenuation of miR124-Sensitive EV-A71 *In Vivo*

The parental and miR124-sensitive EV-A71 virus neurovirulence were evaluated in 1-day-old BALB/c suckling mice or 5- to 6-week-old

female CD-1 nu/nu mice (strain CD-1-Foxn1 nu/Crl; Vital River Laboratory Animal Technology) by intracerebral inoculation, as described previously.[49] Briefly, a single dose of vehicle or 10^7 TCID50s of EV-A71 BrCr or EV-A71-miR124T, diluted in 20 μL of vehicle, was injected into the brains of mice (n = 6–8/group) using a Hamilton syringe. The mice were then monitored for morbidity and mortality up to 14 days postinoculation. To study virus replication, the brains of mice in each group were harvested at the indicated time points, and virus titers in the brain suspensions were quantified by titration in Vero cells.

In Vivo Studies in a Subcutaneous Glioma Model

For subcutaneous tumor xenografting, 2×10^6 U87 cells suspended in 100 μL of PBS were implanted into the right flank of 5- to 6-week-old female CD-1 nu/nu mice. When the tumors reached an average volume of 100 mm^3, the animals were randomized into three groups and injected with a single dose of vehicle or 10^7 TCID50s of EV-A71 BrCr or EV-A71-miR124T diluted in vehicle (100 μL) (n = 6–8/group). Tumor development was monitored, and tumor size was measured every 3rd or 4th day post-treatment using a hand-held caliper. The tumor volume was calculated with the following formula: (largest diameter × smallest diameter^2) × 0.52, as previously described.[51] All animals were monitored closely for possible neurologic disorders, with body weight recorded throughout the experiment to evaluate gross toxicity. The animals were sacrificed by cervical dislocation once the implanted tumor size exceeded 15 mm in any direction, which was considered the humane endpoint of survival data.

In Vivo Studies in an Intracranial Glioma Model

To establish intracranial tumors, 5- to 6-week-old female CD-1 nu/nu mice were anesthetized by intraperitoneal injection of Avertin (2, 2, 2-tribromoethanol; Sigma; 200 mg/kg) and then stereotactically injected with 3×10^5 U87 cells in 3 μL of MEM into the right striatum (1.5–2 mm to the right of the midline and 0.5–1 mm posterior to the coronal suture at a 3-mm depth) using a 30-gauge Hamilton syringe. The incision site was sealed by Vetbond (3M). Previous studies demonstrated that this dose of cells would result in the reliable establishment of solid intracranial gliomas with a tumor volume ranging from approximately 0.5 mm^3 to 1.1 mm^3 on day 7 postimplantation.[46,47] Then, a single dose of virus (10^5 TCID50s) was injected intratumorally using the same coordinates as for tumor cell implantation. Corresponding control groups received vehicle in place of virus (n = 6–8/group). Animals were sacrificed when they lost 20% of their body weight or had difficulty feeding, grooming, or ambulating.

Histology

Animals were anesthetized and perfused intracardially with PBS followed by 4% (w/v) PFA in PBS. Tumors (or remaining masses) or brain tissues were fixed in 4% (w/v) PFA and then trimmed and embedded in paraffin wax. Serial sections were stained with H&E for histological analysis. Slides were analyzed using a Pannoramic Digital Slide Scanner (3DHistech).

IHC

For IHC, the sections were incubated with primary rabbit anti-EV-A71 2B antibody (GTX132343; GeneTex), followed by reaction with horseradish peroxidase-conjugated anti-rabbit IgG secondary antibody (ab7090; Abcam). Slides were then subjected to avidin-biotin complex (ABC), followed by diaminobenzidine (DAB) and hematoxylin counterstaining (Servicebio).

TUNEL

Apoptotic cells in tissue sections were detected by TUNEL staining, using the *In Situ* Cell Death Detection Kit-POD (Roche), according to the manufacturer's instructions. Hematoxylin was used as a counterstain. The appearance of brown-stained cells indicated apoptosis.

FISH-Based miR124 Detection

Brain sections were used for detecting miR124 using the LNA miRCURY probe (Exiqon) labeled with digoxigenin (DIG), as described previously.[52,53] Positive *in situ* hybridization signals were detected by incubation with the anti-DIG primary antibody (ab76907; Abcam), followed by FITC-conjugated secondary antibody (ab97104; Abcam). Nuclei were stained with 4′,6-diamidino-2-phenylindole (DAPI).

Statistical Analyses

Values are expressed as mean ± standard deviations. Unpaired t tests were used, as indicated for two-group comparisons. Statistical analyses were performed using SigmaPlot 10.0 (Systat Software) and GraphPad Prism 5.0 (GraphPad Software), and p values of less than 0.05 were considered statistically significant. All statistical tests were two sided. Survival curves were plotted according to the Kaplan-Meier method, and the groups were compared using log rank tests.

SUPPLEMENTAL INFORMATION

Supplemental Information can be found online at https://doi.org/10.1016/j.ymthe.2020.04.005.

AUTHOR CONTRIBUTIONS

X.Z. conducted the experiments and analyzed the data. Z.C. designed and supervised the research. H.W., Z.Z., and X.-E.Z. participated in data analysis and contributed to editing the manuscript. Y.S. and M.Q. contributed with some experiments. W.L. helped with imaging experiments. X.Z. and Z.C. coordinated the study and wrote the manuscript.

CONFLICTS OF INTEREST

The authors declare no competing interests.

ACKNOWLEDGMENTS

We are grateful to Ding Gao, Juan Min, Fan Zhang, Li Li, and He Zhao from the Core Facility and Technical Support, Wuhan Institute of Virology, for their excellent technical assistance. This work was supported by the Strategic Priority Research Program of the Chinese Academy of Sciences (XDB29050201), National Natural Science

Foundation of China (31400158, 31925025, and 91859108), and Key Research Project of Frontier Science of the Chinese Academy of Sciences (Y703041YZ1).

REFERENCES

1. Osuka, S., and Van Meir, E.G. (2017). Overcoming therapeutic resistance in glioblastoma: the way forward. J. Clin. Invest. *127*, 415–426.
2. Wen, P.Y., and Kesari, S. (2008). Malignant gliomas in adults. N. Engl. J. Med. *359*, 492–507.
3. Omuro, A., and DeAngelis, L.M. (2013). Glioblastoma and other malignant gliomas: a clinical review. JAMA *310*, 1842–1850.
4. Russell, S.J., Peng, K.W., and Bell, J.C. (2012). Oncolytic virotherapy. Nat. Biotechnol. *30*, 658–670.
5. Kelly, E., and Russell, S.J. (2007). History of oncolytic viruses: genesis to genetic engineering. Mol. Ther. *15*, 651–659.
6. Desjardins, A., Gromeier, M., Herndon, J.E., 2nd, Beaubier, N., Bolognesi, D.P., Friedman, A.H., Friedman, H.S., McSherry, F., Muscat, A.M., Nair, S., et al. (2018). Recurrent Glioblastoma Treated with Recombinant Poliovirus. N. Engl. J. Med. *379*, 150–161.
7. Forsyth, P.A., and Abate-Daga, D. (2018). Oncolytic Virotherapy for Malignant Gliomas. J. Clin. Oncol. *36*, 1440–1442.
8. Solomon, T., Lewthwaite, P., Perera, D., Cardosa, M.J., McMinn, P., and Ooi, M.H. (2010). Virology, epidemiology, pathogenesis, and control of enterovirus 71. Lancet Infect. Dis. *10*, 778–790.
9. Buenz, E.J., and Howe, C.L. (2006). Picornaviruses and cell death. Trends Microbiol. *14*, 28–36.
10. Evans, D.J. (1999). Reverse genetics of picornaviruses. Adv. Virus Res. *53*, 209–228.
11. Zhang, X., Zheng, Z., Shu, B., Liu, X., Zhang, Z., Liu, Y., Bai, B., Hu, Q., Mao, P., and Wang, H. (2013). Human astrocytic cells support persistent coxsackievirus B3 infection. J. Virol. *87*, 12407–12421.
12. Yamayoshi, S., Yamashita, Y., Li, J., Hanagata, N., Minowa, T., Takemura, T., and Koike, S. (2009). Scavenger receptor B2 is a cellular receptor for enterovirus 71. Nat. Med. *15*, 798–801.
13. Yamayoshi, S., Iizuka, S., Yamashita, T., Minagawa, H., Mizuta, K., Okamoto, M., Nishimura, H., Sanjoh, K., Katsushima, N., Itagaki, T., et al. (2012). Human SCARB2-dependent infection by coxsackievirus A7, A14, and A16 and enterovirus 71. J. Virol. *86*, 5686–5696.
14. Timmer, J.C., and Salvesen, G.S. (2007). Caspase substrates. Cell Death Differ. *14*, 66–72.
15. Oda, E., Ohki, R., Murasawa, H., Nemoto, J., Shibue, T., Yamashita, T., Tokino, T., Taniguchi, T., and Tanaka, N. (2000). Noxa, a BH3-only member of the Bcl-2 family and candidate mediator of p53-induced apoptosis. Science *288*, 1053–1058.
16. Kelly, E.J., Hadac, E.M., Greiner, S., and Russell, S.J. (2008). Engineering microRNA responsiveness to decrease virus pathogenicity. Nat. Med. *14*, 1278–1283.
17. Wei, J., Wang, F., Kong, L.Y., Xu, S., Doucette, T., Ferguson, S.D., Yang, Y., McEnery, K., Jethwa, K., Gjyshi, O., et al. (2013). miR-124 inhibits STAT3 signaling to enhance T cell-mediated immune clearance of glioma. Cancer Res. *73*, 3913–3926.
18. He, F., Yao, H., Wang, J., Xiao, Z., Xin, L., Liu, Z., Ma, X., Sun, J., Jin, Q., and Liu, Z. (2015). Coxsackievirus B3 engineered to contain microRNA targets for muscle-specific microRNAs displays attenuated cardiotropic virulence in mice. J. Virol. *89*, 908–916.
19. Brostoff, T., Pesavento, P.A., Barker, C.M., Kenney, J.L., Dietrich, E.A., Duggal, N.K., Bosco-Lauth, A.M., and Brault, A.C. (2016). MicroRNA reduction of neuronal West Nile virus replication attenuates and affords a protective immune response in mice. Vaccine *34*, 5366–5375.
20. Liu, M.L., Lee, Y.P., Wang, Y.F., Lei, H.Y., Liu, C.C., Wang, S.M., Su, I.J., Wang, J.R., Yeh, T.M., Chen, S.H., and Yu, C.K. (2005). Type I interferons protect mice against enterovirus 71 infection. J. Gen. Virol. *86*, 3263–3269.
21. Yu, C.K., Chen, C.C., Chen, C.L., Wang, J.R., Liu, C.C., Yan, J.J., and Su, I.J. (2000). Neutralizing antibody provided protection against enterovirus type 71 lethal challenge in neonatal mice. J. Biomed. Sci. *7*, 523–528.
22. Makeyev, E.V., Zhang, J., Carrasco, M.A., and Maniatis, T. (2007). The MicroRNA miR-124 promotes neuronal differentiation by triggering brain-specific alternative pre-mRNA splicing. Mol. Cell *27*, 435–448.
23. Yeom, K.H., Mitchell, S., Linares, A.J., Zheng, S., Lin, C.H., Wang, X.J., Hoffmann, A., and Black, D.L. (2018). Polypyrimidine tract-binding protein blocks miRNA-124 biogenesis to enforce its neuronal-specific expression in the mouse. Proc. Natl. Acad. Sci. USA *115*, E11061–E11070.
24. Wollmann, G., Rogulin, V., Simon, I., Rose, J.K., and van den Pol, A.N. (2010). Some attenuated variants of vesicular stomatitis virus show enhanced oncolytic activity against human glioblastoma cells relative to normal brain cells. J. Virol. *84*, 1563–1573.
25. Jhawar, S.R., Thandoni, A., Bommareddy, P.K., Hassan, S., Kohlhapp, F.J., Goyal, S., Schenkel, J.M., Silk, A.W., and Zloza, A. (2017). Oncolytic Viruses-Natural and Genetically Engineered Cancer Immunotherapies. Front. Oncol. *7*, 202.
26. Polisetty, R.V., Gautam, P., Sharma, R., Harsha, H.C., Nair, S.C., Gupta, M.K., Uppin, M.S., Challa, S., Puligopu, A.K., Ankathi, P., et al. (2012). LC-MS/MS analysis of differentially expressed glioblastoma membrane proteome reveals altered calcium signaling and other protein groups of regulatory functions. Mol. Cell. Proteomics *11*, M111.013565.
27. Nishimura, Y., Shimojima, M., Tano, Y., Miyamura, T., Wakita, T., and Shimizu, H. (2009). Human P-selectin glycoprotein ligand-1 is a functional receptor for enterovirus 71. Nat. Med. *15*, 794–797.
28. Nishimura, Y., Lee, H., Hafenstein, S., Kataoka, C., Wakita, T., Bergelson, J.M., and Shimizu, H. (2013). Enterovirus 71 binding to PSGL-1 on leukocytes: VP1-145 acts as a molecular switch to control receptor interaction. PLoS Pathog. *9*, e1003511.
29. Chen, L.C., Shyu, H.W., Chen, S.H., Lei, H.Y., Yu, C.K., and Yeh, T.M. (2006). Enterovirus 71 infection induces Fas ligand expression and apoptosis of Jurkat cells. J. Med. Virol. *78*, 780–786.
30. Sarkaria, J.N., Kitange, G.J., James, C.D., Plummer, R., Calvert, H., Weller, M., and Wick, W. (2008). Mechanisms of chemoresistance to alkylating agents in malignant glioma. Clin. Cancer Res. *14*, 2900–2908.
31. Liu, L.W., Nishikawa, T., and Kaneda, Y. (2016). An RNA Molecule Derived From Sendai Virus DI Particles Induces Antitumor Immunity and Cancer Cell-selective Apoptosis. Mol. Ther. *24*, 135–145.
32. Kelly, K.R., Espitia, C.M., Mahalingam, D., Oyajobi, B.O., Coffey, M., Giles, F.J., Carew, J.S., and Nawrocki, S.T. (2012). Reovirus therapy stimulates endoplasmic reticular stress, NOXA induction, and augments bortezomib-mediated apoptosis in multiple myeloma. Oncogene *31*, 3023–3038.
33. Qin, J.Z., Ziffra, J., Stennett, L., Bodner, B., Bonish, B.K., Chaturvedi, V., Bennett, F., Pollock, P.M., Trent, J.M., Hendrix, M.J., et al. (2005). Proteasome inhibitors trigger NOXA-mediated apoptosis in melanoma and myeloma cells. Cancer Res. *65*, 6282–6293.
34. Bartel, D.P. (2009). MicroRNAs: target recognition and regulatory functions. Cell *136*, 215–233.
35. Di Leva, G., Garofalo, M., and Croce, C.M. (2014). MicroRNAs in cancer. Annu. Rev. Pathol. *9*, 287–314.
36. Brown, B.D., and Naldini, L. (2009). Exploiting and antagonizing microRNA regulation for therapeutic and experimental applications. Nat. Rev. Genet. *10*, 578–585.
37. Xiao, X., Liang, J., Huang, C., Li, K., Xing, F., Zhu, W., Lin, Z., Xu, W., Wu, G., Zhang, J., et al. (2018). DNA-PK inhibition synergizes with oncolytic virus M1 by inhibiting antiviral response and potentiating DNA damage. Nat. Commun. *9*, 4342.
38. Selman, M., Rousso, C., Bergeron, A., Son, H.H., Krishnan, R., El-Sayes, N.A., Varette, O., Chen, A., Le Boeuf, F., Tzelepis, F., et al. (2018). Multi-modal Potentiation of Oncolytic Virotherapy by Vanadium Compounds. Mol. Ther. *26*, 56–69.
39. Lemos de Matos, A., Franco, L.S., and McFadden, G. (2020). Oncolytic Viruses and the Immune System: The Dynamic Duo. Mol. Ther. Methods Clin. Dev. *17*, 349–358.
40. Ricca, J.M., Oseledchyk, A., Walther, T., Liu, C., Mangarin, L., Merghoub, T., Wolchok, J.D., and Zamarin, D. (2018). Pre-existing Immunity to Oncolytic Virus Potentiates Its Immunotherapeutic Efficacy. Mol. Ther. *26*, 1008–1019.

41. Martin, N.T., and Bell, J.C. (2018). Oncolytic Virus Combination Therapy: Killing One Bird with Two Stones. Mol. Ther. *26*, 1414–1422.

42. Luo, M.H., Hannemann, H., Kulkarni, A.S., Schwartz, P.H., O'Dowd, J.M., and Fortunato, E.A. (2010). Human cytomegalovirus infection causes premature and abnormal differentiation of human neural progenitor cells. J. Virol. *84*, 3528–3541.

43. Arita, M., Shimizu, H., Nagata, N., Ami, Y., Suzaki, Y., Sata, T., Iwasaki, T., and Miyamura, T. (2005). Temperature-sensitive mutants of enterovirus 71 show attenuation in cynomolgus monkeys. J. Gen. Virol. *86*, 1391–1401.

44. Morrissy, A.S., Morin, R.D., Delaney, A., Zeng, T., McDonald, H., Jones, S., Zhao, Y., Hirst, M., and Marra, M.A. (2009). Next-generation tag sequencing for cancer gene expression profiling. Genome Res. *19*, 1825–1835.

45. Benjamini, Y., and Yekutieli, D. (2001). The control of the false discovery rate in multiple testing under dependency. Ann. Statist. *29*, 1165–1188.

46. Ashburner, M., Ball, C.A., Blake, J.A., Botstein, D., Butler, H., Cherry, J.M., Davis, A.P., Dolinski, K., Dwight, S.S., Eppig, J.T., et al.; The Gene Ontology Consortium (2000). Gene ontology: tool for the unification of biology. Nat. Genet. *25*, 25–29.

47. Cazanave, S.C., Mott, J.L., Elmi, N.A., Bronk, S.F., Werneburg, N.W., Akazawa, Y., Kahraman, A., Garrison, S.P., Zambetti, G.P., Charlton, M.R., and Gores, G.J. (2009). JNK1-dependent PUMA expression contributes to hepatocyte lipoapoptosis. J. Biol. Chem. *284*, 26591–26602.

48. Matsushima-Miyagi, T., Hatano, K., Nomura, M., Li-Wen, L., Nishikawa, T., Saga, K., Shimbo, T., and Kaneda, Y. (2012). TRAIL and Noxa are selectively upregulated in prostate cancer cells downstream of the RIG-I/MAVS signaling pathway by nonreplicating Sendai virus particles. Clin. Cancer Res. *18*, 6271–6283.

49. Zhang, X., Zheng, Z., Liu, X., Shu, B., Mao, P., Bai, B., Hu, Q., Luo, M., Ma, X., Cui, Z., and Wang, H. (2016). Tick-borne encephalitis virus induces chemokine RANTES expression via activation of IRF-3 pathway. J. Neuroinflammation *13*, 209.

50. He, B., Lin, G.Y., Durbin, J.E., Durbin, R.K., and Lamb, R.A. (2001). The SH integral membrane protein of the paramyxovirus simian virus 5 is required to block apoptosis in MDBK cells. J. Virol. *75*, 4068–4079.

51. Wollmann, G., Tattersall, P., and van den Pol, A.N. (2005). Targeting human glioblastoma cells: comparison of nine viruses with oncolytic potential. J. Virol. *79*, 6005–6022.

52. Chandrasekar, V., and Dreyer, J.L. (2009). microRNAs miR-124, let-7d and miR-181a regulate cocaine-induced plasticity. Mol. Cell. Neurosci. *42*, 350–362.

53. Pena, J.T., Sohn-Lee, C., Rouhanifard, S.H., Ludwig, J., Hafner, M., Mihailovic, A., Lim, C., Holoch, D., Berninger, P., Zavolan, M., and Tuschl, T. (2009). miRNA in situ hybridization in formaldehyde and EDC-fixed tissues. Nat. Methods *6*, 139–141.